2020 IEEE 17th International Symposium on Biomedical Imaging (ISBI)
April 3-7, 2020, Iowa City, Iowa, USA

HESSIAN SPLINES FOR SCANNING TRANSMISSION X-RAY MICROSCOPY

Thomas Debarre[⋆] *Benjamin Watts*[†] *Benedikt Rösner*[†] *Michael Unser*[⋆]

[⋆] Biomedical Imaging Group, École polytechnique fédérale de Lausanne, Lausanne, Switzerland
[†] Paul Scherrer Institute, Villigen, Switzerland

ABSTRACT

Scanning transmission X-ray microscopy (STXM) produces images in which each pixel value is related to the measured attenuation of an X-ray beam. In practice, the location of the illuminated region does not exactly match the desired uniform pixel grid. This error can be measured using an interferometer. In this paper, we propose a spline-based reconstruction method for STXM which takes these position errors into account. We achieve this by formulating the reconstruction problem as a continuous-domain inverse problem in a spline basis, and by using Hessian nuclear-norm regularization. We solve this problem using the standard ADMM algorithm, and we demonstrate the pertinence of our approach on both simulated and real STXM data.

Index Terms— STXM, inverse problems, splines, interpolation, Hessian nuclear-norm regularization

1. INTRODUCTION

Scanning transmission X-ray microscopy (STXM) is a non-invasive microscopy technique that uses X-ray spectroscopy to generate contrast based on near-edge X-ray absorption fine structure (NEXAFS) spectroscopy or associated dichroism to quantitatively map material properties such as chemical oxidation state, molecular structure and orientation, and magnetisation at the nanoscale [1]. A Fresnel zone plate is used to focus the X-ray beam onto a small region of the sample (a pixel), and the transmitted beam intensity is measured while the sample is raster-scanned in a rectangular array in order to produce a 2D image. With recent advances in the design of the zone plate, X-ray spot sizes well below 10 nm can be achieved [2]. However, demonstrating STXM images with a resolution below 10 nm also requires similarly high precision in positioning the X-ray beam on the sample, which is challenging due to vibrations in the instrument. This imprecision leads to an off-the-grid scanning pattern: in fact, when measuring images close to the resolution limit, the displacement error can easily be larger than the spacing between the array points. This error can be measured using a heterodyne laser interferometer, with spatial resolution 0.3 nm. The current state-of-the-art resolution of 7 nm for STXM is thus achieved by regridding the measured intensity values using linear interpolation [3].

In this work, we propose a more elaborate interpolation method using a continuous-domain inverse problem formulation. For discretization purposes, we reconstruct the image as a parametric continuous 2D function using a spline-based generalized interpolation model [4]. We then formulate the image reconstruction task as an optimization problem over the spline coefficients so as to minimize the discrepancy between the measured data and the reconstructed images.

In order to improve the robustness of the reconstruction, we add a regularization term to the cost functional. In effect, this enables us to reduce the effect of the noise in the measurements, as well as the uncertainty in the interferometer measurements. Our algorithm involves a second-order Hessian nuclear-norm regularization, which has been successfully applied to many imaging problems [5–7]. The key feature of this regularization is that it enjoys many advantages of the popular total-variation (TV) semi-norm [8] such as convexity translation, and scale invariance, without suffering from the staircasing effect which typically plagues TV-based methods. As opposed to the purely discrete framework of [5], we compute the Hessian in the continuous domain, which yield a new brand of splines that we coin *Hessian splines*. The resulting optimization problem is solved using the standard ADMM algorithm [9]. We illustrate the effectiveness of our approach on a simulated ground-truth image, by showing that it outperforms linear interpolation used in state-of-the-art STXM reconstructions. We also apply our algorithm to real high-resolution STXM data. Note that our approach is pertinent for any imaging modality with nonuniform measurements in which the displacement error is nonnegligible.

2. IMAGING MODEL

In this work, we view 2D images as continuous-domain functions $f : \Omega \to \mathbb{R}$, where $\Omega \subset \mathbb{R}^2$ is the (bounded) image domain. Without loss of generality, we assume that the pixels are located on the integer grid, *i.e.*, $\Omega \cap \mathbb{Z}^2$.

2.1. Reconstruction Basis

Following the generalized interpolation approach of [4], we parametrize the reconstructed signal $f : \Omega \to \mathbb{R}$ in a spline basis as

$$f(\boldsymbol{x}) = \sum_{\boldsymbol{k} \in \Omega_\varphi} c[\boldsymbol{k}] \varphi(\boldsymbol{x} - \boldsymbol{k}), \tag{1}$$

where $\boldsymbol{x} = (x_1, x_2) \in \mathbb{R}^2$, $(c[\boldsymbol{k}])_{\boldsymbol{k} \in \Omega_\varphi}$ are the spline coefficients and φ is a suitable spline generating function. The domain $\Omega_\varphi = \{\boldsymbol{k} \in \mathbb{Z}^2 : \mathrm{Supp}(\varphi(\cdot - \boldsymbol{k})) \cap \Omega \neq \emptyset\}$ simply selects the integer grid points $\boldsymbol{k}$ such that the support of the corresponding basis function $\varphi(\cdot - \boldsymbol{k})$ intersects the image domain Ω. In this work, we choose the tensor-product cubic B-spline $\varphi(\boldsymbol{x}) = \beta^3(x_1)\beta^3(x_2)$, where the

The work of T. Debarre and M. Unser is supported by the Swiss National Science Foundation, Grant 200020_184646 / 1. This work uses data from the PolLux beamline of the Swiss Light Source. The PolLux end station was financed by the German Ministerium für Bildung und Forschung (BMBF) through contracts 05KS4WE1/6 and 05KS7WE1.

univariate cubic B-spline is defined as

$$\beta^3(x) = \begin{cases} \frac{2}{3} - |x|^2 + \frac{|x|^3}{2}, & 0 \le |x| < 1 \\ \frac{(2-|x|)^3}{6}, & 1 \le |x| < 2 \\ 0, & \text{otherwise.} \end{cases} \quad (2)$$

Our choice of cubic B-splines is motivated by their simplicity and their popularity in applications [10–13], in part due to their short support. Moreover, they are twice differentiable, which is required to compute the Hessian of f. Since the basis function φ is supported in a square of size 4×4, there is a finite number of spline coefficients $c[\boldsymbol{k}]$ such that $\boldsymbol{k} \in \Omega_\varphi$. We denote these coefficients by $\boldsymbol{c} \in \mathbb{R}^N$, where $N = \#\Omega_\varphi$ (the cardinality of the set).

2.2. Forward Model

In STXM imaging, the task is to reconstruct a continuous-domain function $f_0 : \Omega \to \mathbb{R}$ (the ground-truth image) based on the measured data $\boldsymbol{y} \in \mathbb{R}^M$, where M is the number of measurements, *i.e.*, pixels. The data are acquired via the forward model $\mathrm{A} : f \mapsto (f(\boldsymbol{t}^1), \dots, f(\boldsymbol{t}^M)) \in \mathbb{R}^M$, where $\boldsymbol{t}^m = (t_1^m, t_2^m) \in \mathbb{R}^2$ are the sampling locations measured by the interferometer. The data is corrupted by some additive noise $\boldsymbol{n} \in \mathbb{R}^M$, so that $\boldsymbol{y} = \mathrm{A}\{f_0\} + \boldsymbol{n}$.

Using the parametrization (1) and due to the linearity of A, we specify the discrete forward model by the matrix $\mathbf{A} \in \mathbb{R}^{M \times N}$ such that $\mathbf{A}\boldsymbol{c} = \mathrm{A}\{f\}$, where the vector $\boldsymbol{c} \in \mathbb{R}^N$ collects the spline coefficients of f. Note that if the pixel grid used for the reconstruction is the same as the one intended by the hardware (which is a natural choice), N is slightly larger than M. This is due to the fact that the length of the support of β^3 is larger than 2, which leads to Ω_φ containing points outside of the image domain near the boundaries, *i.e.*, $\Omega_\varphi \not\subset \Omega$. Since there are more unknowns than data points, the problem is thus ill-posed.

2.3. Regularization

In order to increase the robustness of the reconstruction and to handle its aforementioned ill-posedness, we add a Hessian nuclear-norm regularization term to the cost function. This regularization was first introduced in [5], which proposes a discrete version of the functional $\mathcal{R}(f) = \int_\Omega \|\mathrm{H}\{f\}(\boldsymbol{x})\|_* \mathrm{d}\boldsymbol{x}$, where $\mathrm{H}\{f\}(\boldsymbol{x})$ is the Hessian matrix of f at the location $\boldsymbol{x}$, and $\|\cdot\|_*$ is the nuclear norm (also known as the trace or 1-Schatten norm). The latter is defined as $\|\mathbf{M}\|_* = \sum_d |\sigma(\mathbf{M})_d|$, where the $\sigma(\mathbf{M})_d$ are the singular values of the matrix $\mathbf{M}$. The choice of a second-order differential operator — the Hessian —, as opposed to first-order for TV regularization, is designed to promote piecewise-linear reconstructions. Indeed, planes (*i.e.*, first-order polynomials) induce no regularization cost as their Hessian is zero.

Here, we adapt the purely discrete setting of [5] to our continuous-domain representation (1). More precisely, instead of discretizing the Hessian with finite differences, we compute the continuous Hessian operator in terms of the spline coefficients $\boldsymbol{c}$ of f. However, due to the nonlinearity of the singular value decomposition, computing the analytical expression of $\mathcal{R}(f)$ as a function of the coefficients $\boldsymbol{c}$ proves challenging. However, computing the Hessian of f on the integer grid can be done efficiently with digital filtering using the B-spline kernels $b[k] = (\beta^3(k))_{k\in\mathbb{Z}}$, $b^{(1)}[k] = \left(\frac{\mathrm{d}\beta^3}{\mathrm{d}x}(k)\right)_{k\in\mathbb{Z}}$ and $b^{(2)}[k] = \left(\frac{\mathrm{d}^2\beta^3}{\mathrm{d}x^2}(k)\right)_{k\in\mathbb{Z}}$, defined by their z-transforms $B(z) = \frac{z+4+z^{-1}}{6}$, $B^{(1)}(z) = \frac{z+z^{-1}}{2}$, and $B^{(2)}(z) = z - 2 + z^{-1}$ [14]. This yields the Hessian matrix

$$\mathrm{H}_{\boldsymbol{c}}[\boldsymbol{k}] = \begin{pmatrix} \frac{\partial f(\boldsymbol{k})}{\partial^2 x_1} & \frac{\partial f(\boldsymbol{k})}{\partial x_1 x_2} \\ \frac{\partial f(\boldsymbol{k})}{\partial x_2 x_1} & \frac{\partial f(\boldsymbol{k})}{\partial^2 x_2} \end{pmatrix} = \begin{pmatrix} (c * h_{11})[\boldsymbol{k}] & (c * h_{12})[\boldsymbol{k}] \\ (c * h_{12})[\boldsymbol{k}] & (c * h_{22})[\boldsymbol{k}] \end{pmatrix}, \quad (3)$$

where $\boldsymbol{k} \in \mathbb{Z}^2$, and the $h_{i,j}[\boldsymbol{k}]$ are the tensor-product digital filters $h_{1,1}[\boldsymbol{k}] = b^{(2)}[k_1]b[k_2]$, $h_{1,2}[\boldsymbol{k}] = b^{(1)}[k_1]b^{(1)}[k_2]$ and $h_{2,2}[\boldsymbol{k}] = b[k_1]b^{(2)}[k_2]$. Here, $*$ denotes the 2D discrete convolution. We then approximate the integral with a sum over the pixel values, which yields our discretized regularization functional

$$\mathrm{R}(\boldsymbol{c}) = \sum_{\boldsymbol{k}\in\Omega\cap\mathbb{Z}^2} \sum_{d=1}^{2} |\sigma(\mathrm{H}_{\boldsymbol{c}}[\boldsymbol{k}])_d| \quad (4)$$

Note that we only consider the pixels inside the image domain Ω instead of Ω_φ, which contains additional grid points near the boundaries. This avoids unwanted boundary effects, due to the fact that the reconstructed signal (1) goes to zero near the boundaries. In particular, planes (*i.e.*, first-order polynomials) are not penalized using (4), which is a key desired feature of Hessian nuclear-norm regularization.

2.4. Positivity

Since STXM image represent photon counts which are positive by nature, the reconstructed image should satisfy $f(\boldsymbol{x}) \ge 0$ for any $\boldsymbol{x} \in \Omega$. This positivity constraint does not readily translate into a constraint on the coefficients $\boldsymbol{c}$ of f — for instance, we do not necessarily have $c_n \ge 0$ for all n. A simple and easily-computable surrogate is to impose the positivity on the pixel locations $\Omega \cap \mathbb{Z}^2$. As before, this can be achieved with digital filtering with $f(\boldsymbol{k}) = (c * (b \otimes b))[\boldsymbol{k}]$, where $(b \otimes b)[\boldsymbol{k}] = b[k_1]b[k_2]$ is the tensor-product B-spline filter. We thus impose the positivity constraint on the coefficients $\boldsymbol{k} \in \Omega \cap \mathbb{Z}^2$, which can be written in terms of the matrix $\mathbf{B} \in \mathbb{R}^{P\times N}$ as

$$\mathbf{B}\boldsymbol{c} = (f[\boldsymbol{k}])_{\boldsymbol{k}\in\Omega\cap\mathbb{Z}^2} = \Big(c * (b \otimes b)[\boldsymbol{k}]\Big)_{\boldsymbol{k}\in\Omega\cap\mathbb{Z}^2}, \quad (5)$$

where $P = \#(\Omega \cap \mathbb{Z}^2)$ is the number of pixels. Note that we typically have $P = M$, but this is not a requirement of our method.

3. INVERSE PROBLEM FORMULATION AND ALGORITHM

We now formulate the image reconsctruction task as an optimization problem over the spline coefficients $\boldsymbol{c}$. By piecing together the elements of Section 2, we get the following problem

$$\widetilde{\boldsymbol{c}} \in \underset{\boldsymbol{c}\in\mathbb{R}^N}{\arg\min} \Big\{ \|\mathbf{A}\boldsymbol{c} - \boldsymbol{y}\|_2^2 + \lambda \mathrm{R}(\boldsymbol{c}) + i_{\ge 0}(\mathbf{B}\boldsymbol{c}) \Big\}, \quad (6)$$

where $\lambda > 0$, and $i_{\ge 0}$ is the indicator function defined by

$$i_{\ge 0}(\boldsymbol{x}) = \begin{cases} 0 & \text{if } \forall n,\ x_n \ge 0 \\ +\infty & \text{otherwise.} \end{cases} \quad (7)$$

The first term in (6) is known as the data fidelity term, and ensures that the reconstructed signal conforms with the measured data $\boldsymbol{y}$. The second term is the Hessian nuclear-norm regularization, which tends to promote piecewise-linear reconstructed images. The balance between these two terms is controlled by the regularization parameter $\lambda > 0$, which should be tuned according to the noise level

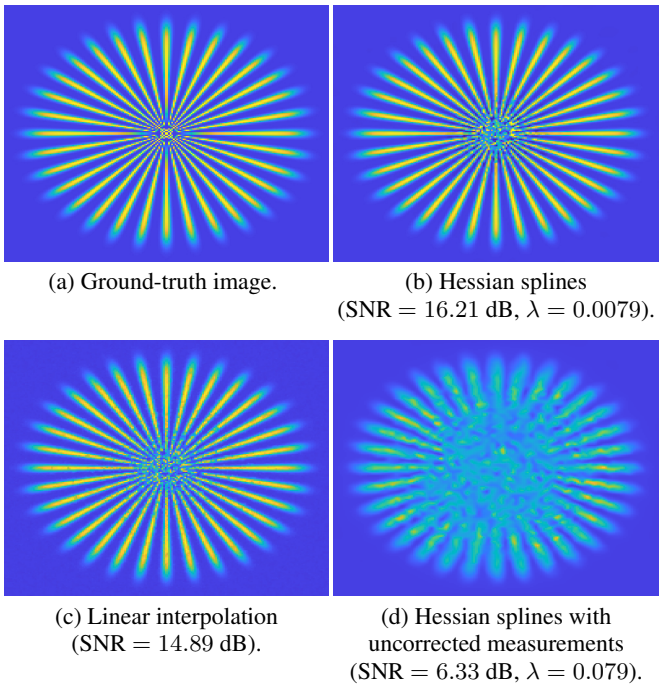

(a) Ground-truth image.

(b) Hessian splines (SNR = 16.21 dB, $\lambda = 0.0079$).

(c) Linear interpolation (SNR = 14.89 dB).

(d) Hessian splines with uncorrected measurements (SNR = 6.33 dB, $\lambda = 0.079$).

Fig. 1: Simulations on a star-like sample.

$\boldsymbol{n}$ and the error in the forward model, *i.e.*, on the sampling locations $\boldsymbol{t}^m$. Finally, the last term in (6) guarantees that the reconstructed image $\widetilde{f}(\boldsymbol{x}) = \sum_{\boldsymbol{k}\in\Omega_\varphi} \widetilde{c}[\boldsymbol{k}]\varphi(\boldsymbol{x}-\boldsymbol{k})$ has positive values at the pixel locations $\boldsymbol{x} \in \Omega \cap \mathbb{Z}^2$.

Despite its somewhat daunting appearance, problem (6) is a convex problem that can be solved with standard proximal algorithms. This is due to the availability of proximal operators for the sum of nulcear norms [5] and for the indicator function $i_{\geq 0}$. We solve it by applying the alternating direction method of multipliers (ADMM) [9], which we implemented in Matlab using GlobalBioIm [15], an inverse-problem library developed at the Biomedical Imaging Group at EPFL. The linear step of ADMM is solved using an inner-loop conjugate gradient (CG) algorithm. Thanks to the modularity of GlobalBioIm, the only block that required implementation was the continuous Hessian operator $(\mathbf{H}(\boldsymbol{k}))_{\boldsymbol{k}\in\Omega_\varphi}$ and its adjoint operator.

Although the theoretical convergence speed of ADMM is rather slow — $\mathcal{O}(k)$, where k is the number of iterations —, in practice, few iterations are necessary to obtain a decent accuracy in few iterations. This is all the more true in STXM due to the availability of a good warm-start initialization for ADMM. The latter can be obtained by computing the spline coefficients of the uncorrected image (*i.e.*, assuming that the measurements are taken on the desired pixel grid) using inverse filtering.

4. EXPERIMENTAL RESULTS

4.1. Simulated Data

In order to assess the pertinence of our Hessian-spline framework, we apply our algorithm to a simulated continuous-domain ground-truth image $f_0 : \mathbb{R}^2 \to [0,1]$, and we evaluate its reconstruction performance in terms of signal-to-noise ratio (SNR). For the ground truth, we use the star-like sample shown in Figure 1 (a), taken from GlobalBioIm. This sample has high-frequency content at the center of the star and lower frequencies towards the end of the branches, and is thus a good benchmarking example. In order to better conform with real STXM images, we add a constant background of 0.1, and we rescale the image so that it ranges from 0.1 to 1.

For the forward model A, the sampling pattern $\boldsymbol{t}^m$, $m = 1,\dots M$ is taken from the real STXM data described in Section 4.2. Note that this pattern is quite far from being uniform: the average displacement with respect to the desired pixel grid is 2.7 nm, which is larger than the pixel size (1 nm). The image size is 200×200, which yields $M = 40000$ measurements. The latter are corrupted by a Poisson noise term $\boldsymbol{n} \in \mathbb{R}^M$, which is applied to the rescaled ground truth image such the maximum pixel value corresponds to the maximum number of photon counts in the real STXM data. We thus have measurements $\boldsymbol{y} = \mathrm{A}\{f_0\} + \boldsymbol{n}$.

We then apply our Hessian-spline algorithm to solve problem (6). The problem dimension is $N = 42436$, which leads to reasonable computations times (in the order of 30 seconds on commodity hardware). For ADMM, we use 5 inner CG iterations . We optimize the regularization parameter λ using grid search in order to maximize the SNR of the reconstructed image with respect to the ground truth f_0. The reconstructed image is shown in Figure 1 (b), and achieves an SNR of 16.21 dB with a regularization parameter $\lambda = 0.0079$.

Next, we compare the performance of Hessian splines with linear interpolation, which is used for achieving the state-of-the-art 7 nm resolution in STXM [3], using the Matlab function "scatteredInterpolant". This method also uses the knowledge of the sampling locations $\boldsymbol{t}^m$, but it does not apply regularization and is therefore more sensitive to noise. The reconstruction image is shown in Figure 1 (c), and achieves an SNR of 14.89 dB.

Finally, we show the effect of the sampling location error by running our algorithm with an uncorrected forward model $\mathrm{A}_{\mathrm{pix}}$, which does not take into account the sampling locations $\boldsymbol{t}^m$ measured by the interferometer. As before, we optimize the regularization parameter using grid search, which yields the reconstructed image shown in Figure 1 (d) and achieves an SNR of 6.33 dB with a regularization parameter $\lambda = 0.079$. We see that the reconstruction fails dramatically, which indicates that using the corrected forward model A is critical in order to achieve good reconstruction results.

4.2. Real Data

We now apply our Hessian spline algorithm to real high-resolution STXM data provided by the Paul Scherrer Institute. The sample being imaged is a grating structure that is part of a Fresnel zone plate. The image size is 200×200 pixels, and the pixel size is 1 nm.

In Figure 2 (a), we show the uncorrected image, assuming that the measurements are taken on the desired pixel grid. Although the effect of the displacement errors is not as glaring as in the simulation in Figure 1 (d), they lead to noticeable jitter artefacts.

In Figure 2 (b), we show our reconstruction results using the corrected sampling locations $\boldsymbol{t}^m$ and the Hessian spline framework with a regularization parameter $\lambda = 5$. Although the reconstruction performance cannot be evaluated quantitatively due to the absence of a ground-truth image, we notice that the jitter artefacts as well as the noise are attenuated, due to the use of the corrected forward model A and the regularization respectively.

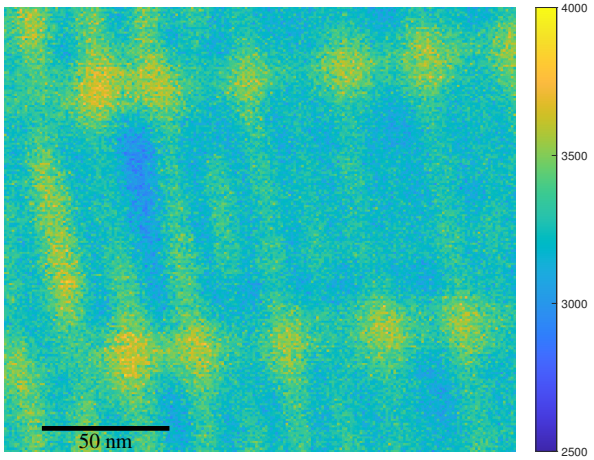

(a) Uncorrected image.

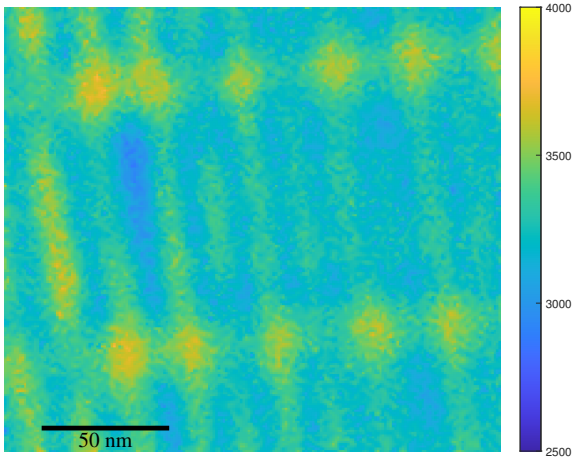

(b) Hessian splines reconstruction with $\lambda = 5$.

Fig. 2: Real STXM data of a grating structure.

5. CONCLUSION

We introduced a new framework, coined as *Hessian splines*, for reconstructing STXM images. This framework takes into account the sampling location errors (*i.e.*, the fact that the measurements are not acquired on a uniform pixel grid), which are measured using an interferometer. We formulated the reconstruction task as a continuous-domain inverse problem with Hessian nuclear-norm regularization. We then discretized the problem in a cubic spline basis, and solved it using ADMM. On the experimental side, we evaluated our method on simulated data, and showed that it outperforms linear interpolation that is used in state-of-the-art high-resolution STXM. We also applied our algorithm to real STXM data.

References

[1] B. Watts and H. Ade, "Nexafs imaging of synthetic organic materials," *Materials Today*, vol. 15, no. 4, pp. 148–157, 2012.

[2] B. Rösner, F. Koch, F. Döring, J. Bosgra, V.A. Guzenko, E. Kirk, M. Meyer, J.L. Ornelas, R.H. Fink, S. Stanescu, et al., "Exploiting atomic layer deposition for fabricating sub-10 nm x-ray lenses," *Microelectronic Engineering*, vol. 191, pp. 91–96, 2018.

[3] B. Rösner, F. Koch, F. Döring, V.A. Guzenko, M. Meyer, J.L. Ornelas, A. Späth, R.H. Fink, S. Stanescu, S. Swaraj, et al., "7 nm spatial resolution in soft x-ray microscopy," *Microscopy and Microanalysis*, vol. 24, no. S2, pp. 272–273, 2018.

[4] M. Unser, "Sampling—50 Years after Shannon," *Proceedings of the IEEE*, vol. 88, no. 4, pp. 569–587, April 2000.

[5] S. Lefkimmiatis, J.P. Ward, and M. Unser, "Hessian Schatten-norm regularization for linear inverse problems," *IEEE Transactions on Image Processing*, vol. 22, no. 5, pp. 1873–1888, May 2013.

[6] S. Lefkimmiatis and M. Unser, "Poisson image reconstruction with Hessian Schatten-norm regularization," *IEEE Transactions on Image Processing*, vol. 22, no. 11, pp. 4314–4327, November 2013.

[7] L. Liu, X. Li, K. Xiang, J. Wang, and S. Tan, "Low-dose CBCT reconstruction using Hessian Schatten penalties," *IEEE Transactions on Medical Imaging*, vol. 36, no. 12, pp. 2588–2599, 2017.

[8] L.I. Rudin, S. Osher, and E. Fatemi, "Nonlinear total variation based noise removal algorithms," *Physica D: nonlinear phenomena*, vol. 60, no. 1-4, pp. 259–268, 1992.

[9] S. Boyd, N. Parikh, E. Chu, B. Peleato, and J. Eckstein, "Distributed optimization and statistical learning via the alternating direction method of multipliers," *Foundations and Trends® in Machine learning*, vol. 3, no. 1, pp. 1–122, 2011.

[10] I.J. Schoenberg, *Cardinal Spline Interpolation*, Philadelphia, PA: SIAM, 1973.

[11] C. De Boor, *A practical guide to splines*, vol. 27, Springer-Verlag, New York, 1978.

[12] M. Unser, "Splines: A perfect fit for signal and image processing," *IEEE Signal Processing Magazine*, vol. 16, no. 6, pp. 22–38, November 1999, IEEE-SPS best paper award.

[13] P. Thévenaz, T. Blu, and M. Unser, "Interpolation revisited," *IEEE Transactions on Medical Imaging*, vol. 19, no. 7, pp. 739–758, July 2000.

[14] M. Unser, A. Aldroubi, and M. Eden, "B-Spline signal processing: Part I—Theory," *IEEE Transactions on Signal Processing*, vol. 41, no. 2, pp. 821–833, February 1993, IEEE-SPS best paper award.

[15] E. Soubies, F. Soulez, M.T. McCann, T.-a. Pham, L. Donati, T. Debarre, D. Sage, and M. Unser, "Pocket guide to solve inverse problems with GlobalBioIm," *Inverse Problems*, vol. 35, no. 10, pp. 1–20, October 2019, paper no. 104006.